Available online at www.sciencedirect.com

ScienceDirect

IFAC PapersOnline CONFERENCE PAPER ARCHIVE

IFAC PapersOnLine 54-16 (2021) 202–207

Adaptive Integral Terminal Sliding Mode Control for an Unmanned Surface Vehicle Against External Disturbances

Alejandro Gonzalez-Garcia * **Herman Castañeda** *

* *Tecnologico de Monterrey, School of Science and Engineering, Av. Eugenio Garza Sada 2501 Sur, 64849 Monterrey, N.L., Mexico. (e-mail: a00818249@itesm.mx, hermancc@tec.mx).*

Abstract: This paper addresses a robust controller for an unmanned surface vehicle subject to external disturbances. An adaptive integral terminal sliding mode technique is designed to control the surge speed and yaw dynamics of the vehicle. Such controller is robust against bounded disturbances, allows finite-time convergence of the tracking error variable, and attenuates the chattering effect common to sliding mode approaches by adapting its control gain. Furthermore, a trajectory tracking guidance law is designed to provide speed and heading references. Simulation results illustrate and compare the advantages and feasibility of the proposed approach in the presence of wind, waves, and currents disturbances.

Keywords: Unmanned surface vehicle, adaptive and robust control, integral terminal sliding mode control, trajectory tracking, maritime robotics

1. INTRODUCTION

Unmanned Surface Vehicles (USVs) operate in different water bodies, such as oceans, coasts, lakes, and rivers, without any onboard crew. The development of fully autonomous surface vehicles can be beneficial for several activities including disaster management (Murphy et al., 2008) and inspection (Lindemuth et al., 2011), among others. Control systems play an important role to ensure safety and success of autonomous operations (Liu et al., 2016). Given the complex nature of the environment where USVs operate, controllers have to be robust against numerous factors such as modeling inaccuracies, unmodeled dynamics, and different unknown external disturbances such as winds, waves, and currents.

Different controllers have been proposed to deal with the complex and nonlinear USV dynamics. For instance, in von Ellenrieder (2018), a backstepping controller with a disturbance observer, capable of operating in the presence of unknown disturbances was proposed. In Klinger et al. (2017), adaptive control was investigated to deal with different displacement and drag configurations. In Huang et al. (2019), a dynamic surface control strategy with active disturbance control was reported. Model-free adaptive control was studied in Liao et al. (2020), showcasing robustness against uncertainties.

A remarkable robust control method is Sliding Mode technique (SMC), which is capable of rejecting bounded perturbations (Shtessel et al., 2014). Therefore, diverse types of SMC have been applied to USV control. In Chen et al. (2019), an SMC heading controller combined with a disturbance observer was developed. One of the common problems of SMC is the so-called chattering effect, which has been attenuated through different methods. Higher-Order SMC and super-twisting SMC approaches reduce chattering, and they were combined in a control-observer scheme in von Ellenrieder and Henninger (2019) for USV trajectory tracking. Another technique is implementing Adaptive SMC (ASMC), which can reduce chattering by avoiding unnecessary control effort with adaptive gains. ASMC was designed and implemented in Gonzalez-Garcia and Castañeda (2021) to control the surge speed and heading of a full-scale USV subject to unknown parametric uncertainties. Faramin et al. (2019) studied ASMC with a disturbance observer for USV control in the presence of wind disturbances. Integral SMC (ISMC) was compared against Adaptive ISMC (AISMC) in Van (2019), where AISMC achieved better performance in the presence of external disturbances.

One disadvantage of conventional SMC is that the tracking error is asymptotically convergent, even if the sliding variable is finite-time convergent. Terminal SMC (TSMC) was developed to overcome this issue. Then, one problem of TSMC is a singularity that appears during control law design. In Wang et al. (2019), a Nonsingular Fast TSMC approach was proposed for trajectory tracking of a USV, capable of handling external disturbances.

Another type of TSMC is Integral TSMC (ITSMC) (Chiu, 2012), which achieves finite-time convergence and avoids the TSMC singularity issue. For conventional SMC, the beneficial properties only appear when the system is on sliding mode (sliding variable equal to zero), making the reaching phase vulnerable to perturbations. A characteristic of ITSMC is that the sliding variable does not have a reaching phase if the initial condition is known. Hence, because the controller is always on sliding mode, the controller is robust even during the tracking error convergence, improving the transient response.

10.1016/j.ifacol.2021.10.094

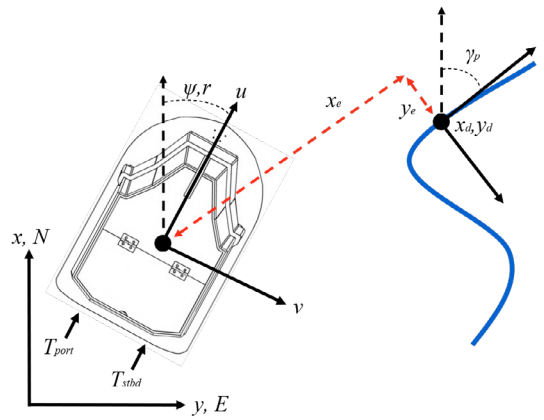

Fig. 1. Reference frames and trajectory tracking problem.

Thus, the contribution of this work is the design of a robust controller for an unmanned surface vehicle subject to wind, waves, and currents. A strategy based on a class of Adaptive Integral Terminal Sliding Mode Control (AITSMC) is designed for the first-order surge speed dynamics and the second-order yaw dynamics. The ITSMC sliding surface guarantees finite-time tracking convergence and enhances robustness during the state reaching phase. The adaptive control gain avoids unnecessary control effort, reducing chattering, and maintains robustness against bounded external perturbations. Moreover, a trajectory tracking guidance law is implemented to provide speed and heading references. Finally, simulation results show the performance and feasibility of the proposed control scheme in the presence of external disturbances from wind, waves, and currents.

The paper is organized as follows: Section 2 presents the dynamic model of the USV and perturbations. Section 3 addresses the design of the controller, whereas Section 4 described the trajectory tracking guidance law. In Section 5, the simulation results are illustrated. Finally, conclusions are drawn.

2. MATHEMATICAL MODELING

In this section, the USV dynamic model and a description of the external perturbations affecting the vehicle are addressed.

2.1 USV dynamic model

The VTec S-III USV model is taken from Gonzalez-Garcia and Castañeda (2021), which follows the robot-like model (Fossen, 2011). The equations of motion are expressed by:

$$\boldsymbol{M}\dot{\boldsymbol{\nu}} + \boldsymbol{C}(\boldsymbol{\nu})\boldsymbol{\nu} + \boldsymbol{D}(\boldsymbol{\nu})\boldsymbol{\nu} = \boldsymbol{\tau} \tag{1}$$

$$\dot{\boldsymbol{\eta}} = \boldsymbol{J}(\boldsymbol{\eta})\boldsymbol{\nu} \tag{2}$$

where $\boldsymbol{\nu} = [u, v, r]^T$ is the velocity vector in body-fixed frame, and $\boldsymbol{\eta} = [x, y, \psi]^T$ is the position vector in an inertial reference frame, where $\psi \in (-\pi, \pi]$. Fig. 1 depicts the USV and its defined reference frames. Then, $\boldsymbol{M}$ represents an inertia matrix including rigid-body and added mass, denoted as:

$$\boldsymbol{M} = \begin{bmatrix} m - X_{\dot{u}} & 0 & -my_G \\ 0 & m - Y_{\dot{v}} & mx_G - Y_{\dot{r}} \\ -my_G & mx_G - N_{\dot{v}} & I_z - N_{\dot{r}}, \end{bmatrix} \tag{3}$$

$\boldsymbol{C}(\boldsymbol{\nu})$ is a Coriolis matrix adding a standard Coriolis rigid-body matrix $\boldsymbol{C}_{RB}(\boldsymbol{\nu})$ and an added mass matrix $\boldsymbol{C}_A(\boldsymbol{\nu})$, being

$$\boldsymbol{C}(\boldsymbol{\nu}) = \begin{bmatrix} 0 & 0 & -m(x_G r + v) \\ 0 & 0 & -m(y_G r - u) \\ m(x_G r + v) & m(y_G r - u) & 0 \end{bmatrix} + \begin{bmatrix} 0 & 0 & 2(Y_{\dot{v}} v + (\frac{Y_{\dot{r}} + N_{\dot{v}}}{2})r) \\ 0 & 0 & -X_{\dot{u}} u \\ 2(-Y_{\dot{v}} v - (\frac{Y_{\dot{r}} + N_{\dot{v}}}{2})r) & X_{\dot{u}} u & 0 \end{bmatrix} \tag{4}$$

Moreover, $\boldsymbol{D}(\boldsymbol{\nu})$ is the sum of linear and nonlinear damping matrices, expressed as follows:

$$\boldsymbol{D}(\boldsymbol{\nu}) = -\begin{bmatrix} X_u & 0 & 0 \\ 0 & Y_v & Y_r \\ 0 & N_v & N_r \end{bmatrix} - \begin{bmatrix} X_{u|u|}|u| & 0 & 0 \\ 0 & Y_{v|v|}|v| + Y_{v|r|}|r| & Y_{r|v|}|v| + Y_{r|r|}|r| \\ 0 & N_{v|v|}|v| + N_{v|r|}|r| & N_{r|v|}|v| + N_{r|r|}|r| \end{bmatrix} \tag{5}$$

while $\boldsymbol{\tau}$ is a vector of forces and moments induced by two rear thrusters, denoted by:

$$\boldsymbol{\tau} = \begin{bmatrix} \tau_u \\ \tau_v \\ \tau_r \end{bmatrix} = \begin{bmatrix} T_{\text{port}} + T_{\text{stbd}} \\ 0 \\ (T_{\text{port}} - T_{\text{stbd}})B/2 \end{bmatrix} \tag{6}$$

The thrusters are saturated between $-30 < T_{\text{port}}, T_{\text{stbd}} < 36.5$ N according to its physical limits (Gonzalez-Garcia and Castañeda, 2021). Finally, $\boldsymbol{J}(\boldsymbol{\eta})$ is a rotation matrix to transform the velocity vectors between body-fixed and inertial reference frames:

$$\boldsymbol{J}(\boldsymbol{\eta}) = \begin{bmatrix} \cos\psi & -\sin\psi & 0 \\ \sin\psi & \cos\psi & 0 \\ 0 & 0 & 1 \end{bmatrix} \tag{7}$$

On the other hand, the physical parameters and hydrodynamic coefficients of the VTec S-III USV can be found in Gonzalez-Garcia and Castañeda (2021), which were previously identified.

2.2 External disturbances modeling

The dynamic model including external disturbances from wind, waves, and currents is expressed in the following form (Fossen, 2011):

$$\boldsymbol{M}\dot{\boldsymbol{\nu}} + \boldsymbol{C}_{RB}(\boldsymbol{\nu})\boldsymbol{\nu} + \boldsymbol{C}_A(\boldsymbol{\nu}_r)\boldsymbol{\nu}_r + \boldsymbol{D}(\boldsymbol{\nu}_r)\boldsymbol{\nu}_r = \boldsymbol{\tau} + \boldsymbol{\tau}_{\text{wind}} + \boldsymbol{\tau}_{\text{wave}} \tag{8}$$

where $\boldsymbol{\nu}_r = \boldsymbol{\nu} - \boldsymbol{\nu}_c$ is the relative velocity and $\boldsymbol{\nu}_c$ is the water current velocity vector, respectively. $\boldsymbol{\tau}_{\text{wind}}$ includes the wind induced forces and moments, and $\boldsymbol{\tau}_{\text{wave}}$ the forces and moments due to waves.

Water currents Such effects are modeled by a Gauss-Markov process (Fossen, 2011), described by:

$$\dot{V}_c + \mu_c V_c = \omega_c \tag{9}$$

where V_c stands the current magnitude, with direction β_c and $\mu_c > 0$, respectively, and ω_c is a Gaussian noise signal. Then, the current velocity vector is then defined for irrotational currents as:

$$\boldsymbol{\nu}_c = \begin{bmatrix} V_c \cos(\beta_c - \psi) \\ V_c \sin(\beta_c - \psi) \\ 0 \end{bmatrix} \tag{10}$$

Waves This kind of perturbations are forces as $F_{\text{wave}} = \sqrt{X_{\text{wave}}^2 + Y_{\text{wave}}^2}$, and moments due to waves N_{wave}, independent to the hull of the USV (Fossen, 2011). They are expressed in state space form as:

$$\begin{bmatrix}\dot{x}_{F1}\\ \dot{x}_{F2}\end{bmatrix} = \begin{bmatrix}0 & 1\\ -\omega_e^2 & -2\lambda_w\omega_e\end{bmatrix}\begin{bmatrix}x_{F1}\\ x_{F2}\end{bmatrix} + \begin{bmatrix}0\\ K_w\end{bmatrix}\omega_{F1} \tag{11}$$

$$F_{\text{wave}} = [0\ 1]\begin{bmatrix}x_{F1}\\ x_{F2}\end{bmatrix} + d_F \tag{12}$$

$$\begin{bmatrix}\dot{x}_{N1}\\ \dot{x}_{N2}\end{bmatrix} = \begin{bmatrix}0 & 1\\ -\omega_e^2 & -2\lambda_w\omega_e\end{bmatrix}\begin{bmatrix}x_{N1}\\ x_{N2}\end{bmatrix} + \begin{bmatrix}0\\ K_w\end{bmatrix}\omega_{N1} \tag{13}$$

$$N_{\text{wave}} = [0\ 1]\begin{bmatrix}x_{N1}\\ x_{N2}\end{bmatrix} + d_N \tag{14}$$

where $K_w > 0$, $\lambda_w > 0, \dot{d}_F = \omega_{F2}, \dot{d}_N = \omega_{N2}$, and $\omega_{F1}, \omega_{F2}, \omega_{N1}, \omega_{N2}$ are Gaussian process signals. ω_e is given by:

$$\omega_e(U, \omega_0, \beta_{\text{wave}}) = \left|\omega_0 - \frac{\omega_0^2}{g} U\cos(\beta_{\text{wave}})\right| \tag{15}$$

with ω_0 as the wave spectrum peak frequency, β_{wave} the wave direction, $g \approx 9.81$ m/s^2 is the gravity, and $U = \sqrt{u^2 + v^2}$. Finally, the wave disturbance vector is:

$$\boldsymbol{\tau}_{\text{wave}} = \begin{bmatrix}X_{\text{wave}}\\ Y_{\text{wave}}\\ N_{\text{wave}}\end{bmatrix} = \begin{bmatrix}F_{\text{wave}}\cos(\beta_{\text{wave}} - \psi)\\ F_{\text{wave}}\sin(\beta_{\text{wave}} - \psi)\\ N_{\text{wave}}\end{bmatrix} \tag{16}$$

Wind The wind effect on the USV can be defined as:

$$\boldsymbol{\tau}_{\text{wind}} = \begin{bmatrix}X_{\text{wind}}\\ Y_{\text{wind}}\\ N_{\text{wind}}\end{bmatrix} = \frac{1}{2}\rho_a V_{rw}^2 \begin{bmatrix}C_X(\gamma_{rw})A_{FW}\\ C_Y(\gamma_{rw})A_{LW}\\ C_N(\gamma_{rw})A_{LW}L_{OA}\end{bmatrix} \tag{17}$$

where $\rho_a \approx 1.2$ kg/m^3 is the air density, $V_{rw} = \sqrt{u_{rw}^2 + v_{rw}^2}$ is the wind relative speed, V_w states the wind velocity, $u_{rw} = u - u_w, v_{rw} = v - v_w, u_w = V_w\cos(\beta_{\text{wind}} - \psi), u_w = V_w\sin(\beta_{\text{wind}} - \psi)$, $\gamma_{rw} = -\text{atan2}(v_{rw}, u_{rw})$ represents the wind angle of attack, β_{wind} is the wind direction, A_{FW} corresponds to the projected frontal area, A_{LW} is the projected lateral area, and L_{OA} is the USV length. The coefficients are computed with:

$$C_X(\gamma_{rw}) = CD_{lAF}\frac{\cos(\gamma_{rw})}{1 - \frac{\delta}{2}(1 - \frac{CD_l}{CD_t})\sin^2(2\gamma_{rw})} \tag{18}$$

$$C_Y(\gamma_{rw}) = CD_t\frac{\sin(\gamma_{rw})}{1 - \frac{\delta}{2}(1 - \frac{CD_l}{CD_t})\sin^2(2\gamma_{rw})} \tag{19}$$

$$C_N(\gamma_{rw}) = -0.18(\gamma_{rw} - \frac{\pi}{2})C_Y(\gamma_{rw}) \tag{20}$$

Considering the VTec S-III USV, it is assumed that $CD_{lAF}(0) = 0.55, CD_{lAF}(\pi) = 0.6, \delta = 0.6, A_{FW} = 0.225, A_{LW} = 0.3, CD_l = CD_{lAF}(\gamma_{rw})A_{FW}/A_{LW}, CD_t = 0.9$.

3. ADAPTIVE INTEGRAL TERMINAL SLIDING MODE

In this section, the design of surge speed and heading control for the USV is presented. To design such controllers, the model (1) is reduced following some assumptions from Gonzalez-Garcia and Castañeda (2021):

- *Assumption 1.* The vehicle is a rigid body, with homogeneous mass distribution, and the shape structure is port/starboard symmetric.
- *Assumption 2.* The body-fixed frame origin is located at the center of gravity of the vessel.
- *Assumption 3.* The heave, pitch, and roll dynamics are neglected on the horizontal plane.
- *Assumption 4.* The off-diagonal terms of inertial and damping matrices are small compared to the main diagonal terms, and hence can be neglected.
- *Assumption 5.* Unmodeled dynamics, parameter inaccuracies, and external disturbances are considered as uncertainties.

Hence, the uncertain model is expressed as:

$$\dot{u} = \frac{1}{m - X_{\dot{u}}}\left[(m - Y_{\dot{v}})vr + X_{u|u|}u|u| + X_u u + \tau_u\right] - \Delta_u \tag{21}$$

$$\dot{v} = X(u, r) + Y(v) - \Delta_v \tag{22}$$

$$\dot{r} = \frac{1}{I_z - N_{\dot{r}}}\left[(-X_{\dot{u}} + Y_{\dot{v}})uv + N_{r|r|}r|r| + N_r r + \tau_r\right] - \Delta_r \tag{23}$$

where

$$X(u, r) = \frac{1}{m - Y_{\dot{v}}}\left[(-m + X_{\dot{u}})ur\right] \tag{24}$$

$$Y(v) = \frac{1}{m - Y_{\dot{v}}}\left[Y_{v|v|}v|v| + Y_v v\right] \tag{25}$$

There is a lack of control input in sway (22) because the USV is underactuated. Thus, $X(u, r)$ and $Y(v)$ are assumed to be bounded by mechanical design such that $Y(v)$ satisfies $Y(v) \leq Y_{min} < 0$ (Paliotta et al., 2019). Δ_u, Δ_v and Δ_r are uncertainties and external disturbances, which are assumed to be both bounded and unknown. Then, a robust control strategy based on AITSMC is proposed to reject these unknown perturbations.

3.1 Surge speed control

Consider the following first-order uncertain system derived from (21):

$$\dot{\xi}_u = f(\xi_u) + g(\xi_u)U_u - \Delta_u \tag{26}$$

where $\xi_u = u$ is the state,

$$f(\xi_u) = \frac{1}{m - X_{\dot{u}}}\left[(m - Y_{\dot{v}})vr + X_{u|u|}u|u| + X_u u\right] \tag{27}$$

$$g(\xi_u) = \frac{1}{m - X_{\dot{u}}} \tag{28}$$

are nonlinear functions, and U_u is the control input. Next, to design the AITSMC, an integral terminal sliding surface is defined as:

$$s_u = e_u + \alpha_u e_{I,u} \tag{29}$$

$$\dot{e}_{I,u} = \text{sign}(e_u)|e_u|^{q_u/p_u} \tag{30}$$

where $e_{I,u}(0) = -e_u(0)/\alpha_u$, $e_u = (u_d - u)$ is the surge speed error, u_d is the desired speed, $\alpha_u > 0$ is a fixed parameter, and p_u and q_u are odd integers satisfying $p_u > q_u > 0$. If s_u is always kept as zero (i.e. $e_u = -\alpha_u e_{I,u}$), then $e_{I,u}$ and e_u are finite-time convergent as proven in Chiu (2012). Next, the time derivative of (30) results in:

$$\begin{aligned}\dot{s}_u &= \dot{e}_u + \alpha_u\dot{e}_{I,u}\\ &= \dot{u}_d - (f(\xi_u) + g(\xi_u)U_u - \Delta_u) + \alpha_u\dot{e}_{I,u}\end{aligned} \tag{31}$$

Hence, one can design the following control $U_u = \tau_u$:

$$\tau_u = \frac{1}{g(\xi_u)}\left[-f(\xi_u) + \dot{u}_d + \alpha_u\dot{e}_{I,u} - u_{a,u}\right] \tag{32}$$

where $u_{a,u}$ is an auxiliary control driven by an adaptive sliding mode strategy:

$$u_{a,u} = -K_{1,u}|s_u|^{(1/2)}\text{sign}(s_u) - K_{2,u}s_u \tag{33}$$

with $K_{1,u}$ computed with the following adaptation law:

$$\dot{K}_{1,u} = \begin{cases} k_{\theta,u}\text{sign}(|s_u| - \mu_u), & \text{if } K_{1,u} > K_{min,u} \\ K_{min,u}, & \text{if } K_{1,u} \leq K_{min,u} \end{cases} \tag{34}$$

and $K_{2,u} > 0$ is a constant parameter. The adaptive controller adjusts $K_{1,u}$ to increase if the sliding variable is larger than threshold $\mu_u > 0$, which detects the loss of sliding mode. If s_u is lower than μ_u, it decreases until reaching $K_{min,u} > 0$, which ensures no zero gain, hence reducing unnecessary control gain, and $k_{\theta,u} > 0$ establishes the gain adaptation rate. Inserting (32) in (31) results in:

$$\dot{s}_u = u_{a,u} + \Delta_u \tag{35}$$

The stability and convergence of this closed-loop was proven in Castañeda et al. (2021).

3.2 Heading control

Now, consider a second-order uncertain system:

$$\begin{aligned} \dot{\xi}_\psi &= \xi_r \\ \dot{\xi}_r &= f(\xi_\psi) + g(\xi_\psi)U_\psi - \Delta_r \end{aligned} \tag{36}$$

where $\xi_\psi = \psi$ is the state, $\xi_r = r$,

$$f(\xi_\psi) = \frac{1}{I_z - N_{\dot{r}}}\left[(-X_{\dot{u}} + Y_{\dot{v}})uv + N_{r|r|}r|r| + N_r r\right] \tag{37}$$

$$g(\xi_\psi) = \frac{1}{I_z - N_{\dot{r}}} \tag{38}$$

are smooth functions, and U_ψ is the control input. Then, the following integral sliding surface for second-order systems is defined as (Wang et al., 2018):

$$s_\psi = \dot{e}_\psi + \beta_\psi e_\psi + \alpha_\psi e_{I,\psi} \tag{39}$$

$$\dot{e}_{I,\psi} = \text{sign}(e_\psi)|e_\psi|^{q_\psi/p_\psi} \tag{40}$$

where $e_{I,\psi}(0) = -[\dot{e}_\psi(0) + \beta_\psi e_\psi(0)]/\alpha_\psi$, $e_\psi \in (-\pi, \pi] = (\psi_d - \psi)$ is the yaw error, $\psi_d \in (-\pi, \pi]$ is the desired heading, $\beta_\psi, \alpha_\psi > 0$, and p_ψ, q_ψ are odd integers which satisfy $p_\psi > q_\psi > 0$. Similar to the first-order case, with $s(0) = 0$, the tracking error was proven to be finite-time convergent (Wang et al., 2018). Then, the derivative of s_ψ with respect to time results in:

$$\begin{aligned} \dot{s}_\psi &= \ddot{e}_\psi + \beta_\psi\dot{e}_\psi + \alpha_\psi\dot{e}_{I,\psi} \\ &= \dot{r}_d - (f(\xi_\psi) + g(\xi_\psi)U_\psi - \Delta_r) + \beta_\psi\dot{e} + \alpha_\psi\dot{e}_{I,\psi} \end{aligned} \tag{41}$$

Thus, the following controller $U_\psi = \tau_r$ is designed:

$$\tau_r = \frac{1}{g(\xi_\psi)}\left[-f(\xi_\psi) + \dot{r}_d + \beta_\psi\dot{e} + \alpha_\psi\dot{e}_{I,\psi} - u_{a,\psi}\right] \tag{42}$$

where $u_{a,\psi}$ follows the adaptive sliding mode technique:

$$u_{a,\psi} = -K_{1,\psi}|s_\psi|^{(1/2)}\text{sign}(s_\psi) - K_{2,\psi}s_\psi \tag{43}$$

where the dynamics of $K_{1,\psi}$ are driven by (34).

4. GUIDANCE LAW

In this section, to compute the desired references u_d and ψ_d for the AITSMC, the trajectory tracking guidance law proposed in Huang et al. (2019) is applied. The procedure

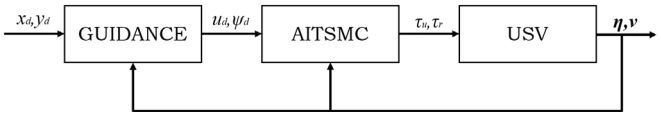

Fig. 2. Guidance-control scheme diagram.

starts by defining the along-track x_e and cross-track y_e errors as follows:

$$\begin{bmatrix} x_e \\ y_e \end{bmatrix} = \begin{bmatrix} \cos\gamma_p & \sin\gamma_p \\ -\sin\gamma_p & \cos\gamma_p \end{bmatrix}\begin{bmatrix} x - x_d \\ y - y_d \end{bmatrix} \tag{44}$$

where x_d and y_d are the desired inertial positions, and $\gamma_p = \text{atan2}(\dot{y}_d, \dot{x}_d)$ is the desired path angle. Then, the desired surge speed is obtained with:

$$u_d = \sqrt{U_{\text{pseudo}}^2 - v^2} \tag{45}$$

where

$$U_{\text{pseudo}} = \frac{(U_d - k_U x_e)\sqrt{y_e^2 + \Delta_L^2}}{\Delta_L} \tag{46}$$

$k_U > 0$ is a constant gain, $\Delta_L > 0$ is a constant look-ahead distance, and $U_d = \sqrt{\dot{x}_d^2 + \dot{y}_d^2}$. Now, the desired heading is computed using:

$$\psi_d = \gamma_p + \text{atan}\left(\frac{-y_e}{\Delta_L}\right) - \beta \tag{47}$$

where $\beta = \text{atan2}(v, u)$ stands for the sideslip angle between the USV and the velocity vector direction. Given that the ITSMC sliding surface is finite-time convergent (Chiu, 2012; Wang et al., 2018), and the ASMC is finite-time convergent (Castañeda et al., 2021), the surge speed and heading errors e_u and e_ψ converge to zero in finite-time. Since convergence of along-track x_e and cross-track y_e errors is guaranteed in Huang et al. (2019), then the guidance-control system is convergent as well. Moreover, a diagram of the scheme is illustrated in Fig. 2, and the trajectory tracking problem is graphically described in Fig. 1.

5. SIMULATION RESULTS

In this section, simulation results to validate the effectiveness and robustness of the proposed control strategy while subject to external disturbances are presented. Simulations were performed in MATLAB/Simulink at a frequency of 100 Hz. First, a test for surge speed and heading control is addressed, then a trajectory tracking case is also evaluated.

5.1 Surge velocity and heading control tests

In this test, the proposed AITSMC was compared against the ASMC from Gonzalez-Garcia and Castañeda (2021) to illustrate the robustness superiority. A reference surge speed of $u_d = 0.7$ m/s was considered, with a time-varying yaw reference of $\psi_d = 0.4\sin(0.1\pi t) + 0.4$ rad for $0 < t < 40$ s. The initial condition was $\boldsymbol{\eta}(0) = \boldsymbol{\nu}(0) = [0, 0, 0]^T$. To verify robustness, external disturbances from currents, waves, and wind were considered with $\mu_c = 0.5$, ω_c with a frequency $f = 20$ Hz and standard deviation $\sigma = 1$ for currents; $K_w = 0.64$, $\lambda_w = 0.1$, $\omega_o = 0.8$, ω_{F1} with $f = 20$ Hz and $\sigma = 10$, ω_{F2} with $f = 20$ Hz and $\sigma = 2$, ω_{N1} with $f = 20$ Hz and $\sigma = 1$, and ω_{N2} with $f = 20$ Hz and $\sigma = 0.1$ for waves; $V_w = 10.28$ m/s for wind; and

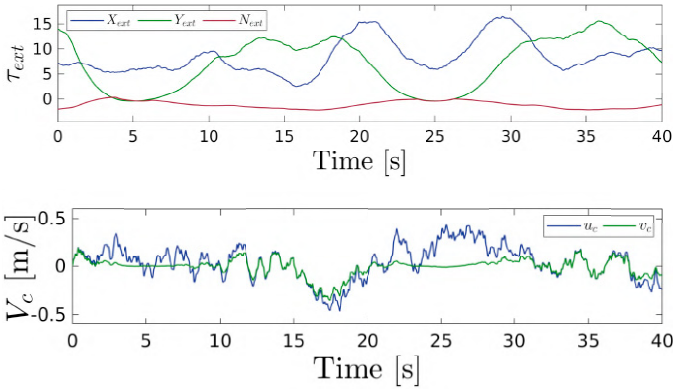

Fig. 3. Applied currents, waves and wind disturbances.

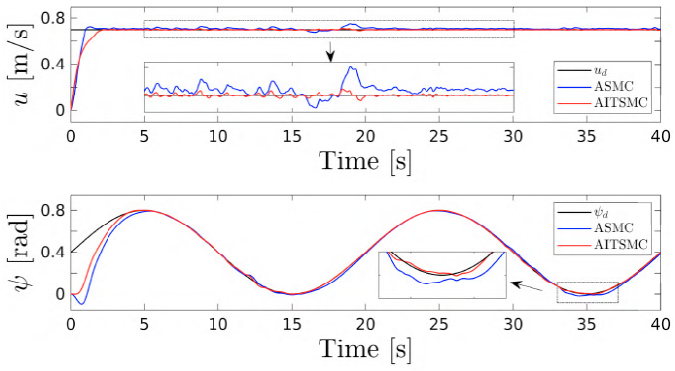

Fig. 4. Surge speed and yaw subject to perturbations.

$\beta_c = \beta_{\text{wave}} = \beta_{\text{wind}} = 0.77$. The resulting behavior can be seen in Fig. 3 in the body-fixed frame. On the other hand, the gains of the AITSMC were set as $\alpha_u = 1$, $q_u = 3$, $p_u = 5$, $k_{\theta,u} = 2$, $\mu_u = 0.01$, $K_{min,u} = 0.1$, $k_{2,u} = 0.1$, $\alpha_\psi = 1$, $\beta_\psi = 3$, $q_\psi = 3$, $p_\psi = 5$, $k_{\theta,\psi} = 2$, $\mu_\psi = 0.01$, $K_{min,\psi} = 0.1$, $k_{2,\psi} = 0.1$.

In Fig. 4, the tracking of surge speed and yaw dynamics is shown to be robust for both controllers, and it is noticeable in both plots how the AITSMC has lower deviations from the reference signals. Hence, the AITSMC is more robust. Additionally, there is no overshoot in the AITSMC responses, which is one of the ITSMC sliding surface characteristics. Likewise, heading responses showcase the added robustness during the reaching phase, as the ASMC deviates to negative ψ values because of the disturbances, and the AITSMC does not. In Fig. 5, the adaptive gains behave similarly for both controllers. The gains remain active throughout the experiment to reject the complex disturbances. In Fig. 6, one difference is during the convergence of the tracking errors, as the ASMC saturates the signal and the AITSMC does not, consequence of the improved transient response induced by the ITSMC sliding surface.

5.2 Trajectory tracking

A second experiment considered the trajectory tracking scenario, where the guidance law from Section 4 is evaluated with the AITSMC. The reference trajectory was designed as $x_d = 10\sin(0.02\pi t)$ and $y_d = -20\cos(0.01\pi t) + 21.5$ for $0 \leq t \leq 200$ s. Such trajectory has a time-varying

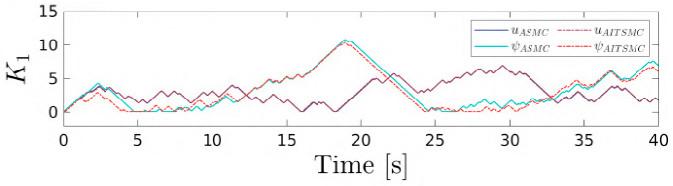

Fig. 5. Evolution of AITSMC and ASMC adaptive gains.

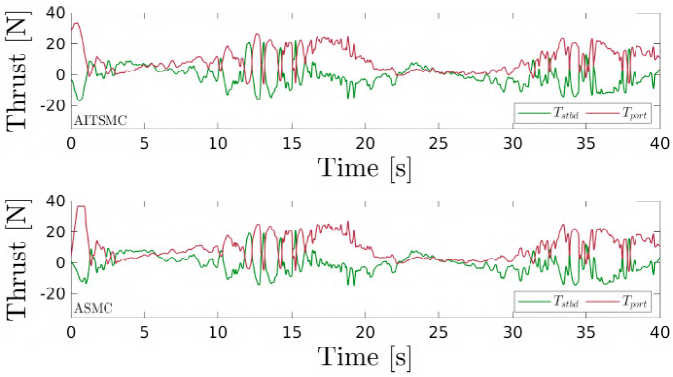

Fig. 6. Control input signals

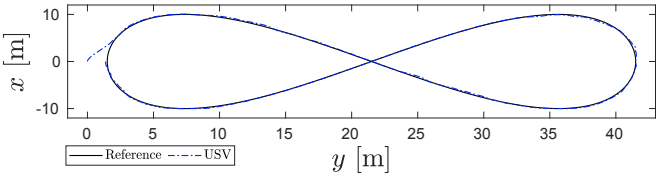

Fig. 7. Desired versus USV Trajectory.

curvature and allows to see the disturbance affecting the USV from different angles. The initial conditions were the same as in the previous experiment, and the external disturbances were equal with the exception of $V_w = 5.11$ and V_c was multiplied by 0.5. These changes were introduced to avoid unmatched disturbances in some segments of the trajectory. Nonetheless, the disturbances were still highly complex for the VTec S-III USV. The parameters for the guidance law were $k_U = 0.1$ and $\Delta_L = 1$. Additionally, u_d is limited by:

$$u_d = \begin{cases} u_d, & \text{if } u_d \leq 1 \\ 1, & \text{if } u_d > 1 \end{cases} \tag{48}$$

In Fig. 7 the USV trajectory is shown to be robust and effective at following the reference trajectory, while subject to external disturbances. In Fig. 8, the output of the guidance law is shown as the desired values for the AITSMC surge speed and yaw controllers. Once again, the robustness of the AITSMC controller is showcased by accurately following the time-varying references in presence of perturbations. In Fig. 9, the gains are depicted to be rejecting disturbances throughout the experiment. Likewise, the control signals, although very active because of the perturbations, are feasible by the physical system.

6. CONCLUSIONS

A robust controller based on adaptive integral terminal sliding mode for an unmanned surface vehicle subject to external disturbances has been proposed. Such perturbations were induced as water currents, waves, and

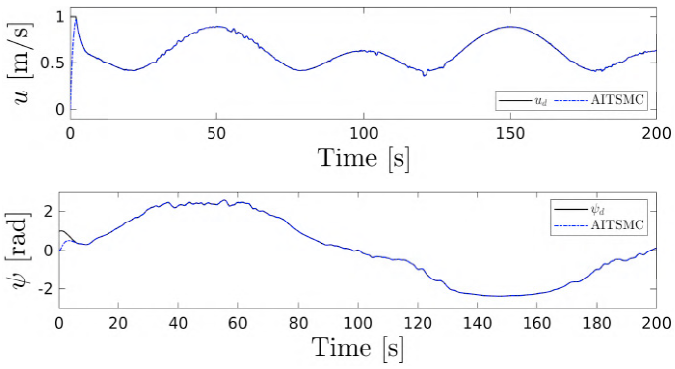

Fig. 8. Surge speed and yaw responses.

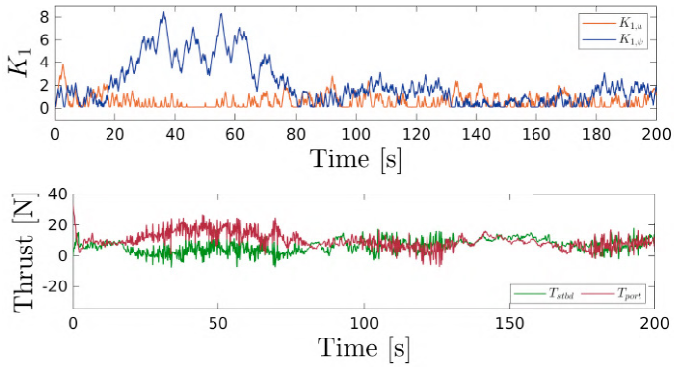

Fig. 9. Adaptive gains and control signals.

wind. Surge speed and heading controllers based on the AITSMC exhibited accuracy and rejection of such adverse effects. The integral terminal sliding surface guaranteed finite-time state convergence, enhanced robustness, and improved the transient response by eliminating the sliding variable reaching phase. For the trajectory tracking scenario, a guidance law was included to provide the desired references. Finally, simulation results of tracking of time-varying references, and trajectory tracking subject to disturbances illustrated and compared the improved accuracy and robustness of the proposed controller.

REFERENCES

Castañeda, H., Rodriguez, J., and Gordillo, J.L. (2021). Continuous and smooth differentiator based on adaptive sliding mode control for a quad-rotor MAV. *Asian Journal of Control*, 23(2), 661–672.

Chen, Z., Zhang, Y., Zhang, Y., Nie, Y., Tang, J., and Zhu, S. (2019). Disturbance-observer-based sliding mode control design for nonlinear unmanned surface vessel with uncertainties. *IEEE Access*, 7, 148522–148530.

Chiu, C.S. (2012). Derivative and integral terminal sliding mode control for a class of mimo nonlinear systems. *Automatica*, 48(2), 316–326.

Faramin, M., Goudarzi, R., and Maleki, A. (2019). Track-keeping observer-based robust adaptive control of an unmanned surface vessel by applying a 4-dof maneuvering model. *Ocean Engineering*, 183, 11 – 23.

Fossen, T.I. (2011). *Handbook of Marine Craft Hydrodynamics and Motion Control*. John Wiley & Sons.

Gonzalez-Garcia, A. and Castañeda, H. (2021). Guidance and control based on adaptive sliding mode strategy for a usv subject to uncertainties. *IEEE Journal of Oceanic Engineering*, 1–11. doi:10.1109/JOE.2021.3059210.

Huang, H., Gong, M., Zhuang, Y., Sharma, S., and Xu, D. (2019). A new guidance law for trajectory tracking of an underactuated unmanned surface vehicle with parameter perturbations. *Ocean Engineering*, 175, 217 – 222.

Klinger, W.B., Bertaska, I.R., von Ellenrieder, K.D., and Dhanak, M.R. (2017). Control of an unmanned surface vehicle with uncertain displacement and drag. *IEEE Journal of Oceanic Engineering*, 42(2), 458–476.

Liao, Y., Jiang, Q., Du, T., and Jiang, W. (2020). Redefined output model-free adaptive control method and unmanned surface vehicle heading control. *IEEE Journal of Oceanic Engineering*, 45(3), 714–723.

Lindemuth, M., Murphy, R., Steimle, E., Armitage, W., Dreger, K., Elliot, T., Hall, M., Kalyadin, D., Kramer, J., Palankar, M., Pratt, K., and Griffin, C. (2011). Sea robot-assisted inspection. *IEEE Robotics Automation Magazine*, 18(2), 96–107.

Liu, Z., Zhang, Y., Yu, X., and Yuan, C. (2016). Unmanned surface vehicles: An overview of developments and challenges. *Annual Reviews in Control*, 41, 71 – 93.

Murphy, R.R., Steimle, E., Griffin, C., Cullins, C., Hall, M., and Pratt, K. (2008). Cooperative use of unmanned sea surface and micro aerial vehicles at hurricane wilma. *Journal of Field Robotics*, 25(3), 164–180.

Paliotta, C., Lefeber, E., Pettersen, K.Y., Pinto, J., Costa, M., and de Figueiredo Borges de Sousa, J.T. (2019). Trajectory tracking and path following for underactuated marine vehicles. *IEEE Transactions on Control Systems Technology*, 27(4), 1423–1437.

Shtessel, Y., Edwards, C., Fridman, L., and Levant, A. (2014). *Sliding Mode Control and Observation*. Birkhäuser Basel.

Van, M. (2019). An enhanced tracking control of marine surface vessels based on adaptive integral sliding mode control and disturbance observer. *ISA Transactions*, 90, 30–40.

von Ellenrieder, K.D. (2018). Stable backstepping control of marine vehicles with actuator rate limits and saturation. *IFAC-PapersOnLine*, 51(29), 262–267.

von Ellenrieder, K.D. and Henninger, H.C. (2019). A higher order sliding mode controller-observer for marine vehicles. *IFAC-PapersOnLine*, 52(21), 341–346.

Wang, H., Li, Z., Jin, X., Huang, Y., Kong, H., Yu, M., Ping, Z., and Sun, Z. (2018). Adaptive integral terminal sliding mode control for automobile electronic throttle via an uncertainty observer and experimental validation. *IEEE Transactions on Vehicular Technology*, 67(9), 8129–8143.

Wang, N., Karimi, H.R., Li, H., and Su, S. (2019). Accurate trajectory tracking of disturbed surface vehicles: A finite-time control approach. *IEEE/ASME Transactions on Mechatronics*, 24(3), 1064–1074.